JOURNAL OF SOLID STATE CHEMISTRY 89, 237–259 (1990)

A Study of the System Yb + S, Mainly by Electron Diffraction/Microscopy

L. C. OTERO-DÍAZ, A. R. LANDA-CÁNOVAS, AND B. G. HYDE*

Química Inorgánica, F. Químicas, Universidad Complutense, 28040 Madrid, Spain

Received March 23, 1990

An electron diffraction study of various ytterbium sulfide preparations reveals the presence of several phases: "Yb_3S_4" in two orthorhombic forms, *Ccmm* at high temperatures and *Pnma*, the latter sometimes incommensurately modulated, sometimes not; B1-related types, both cubic and rhombohedral, again the latter sometimes incommensurately modulated. The results are generally consistent with those previously reported. They reveal the absence of long-range order in some of the B1-related phases, and the consequent difficulty in identifying and delineating the phase relations between the cubic and rhombohedral $Yb_{1-\delta}S$ types.

Introduction

In the binary system Yb + S several phases have been reported by Flahaut's group (*1–4*), in order of decreasing sulfur content: (i) A stoichiometric sesquisulfide, Yb_2S_3, which is polymorphic: rhombohedral, corundum type above 1200°C, and cubic, bixbyite type (= Tl_2O_3 = rare earth C-type sesquioxide) at 850°C. (*5*). (ii) A widely nonstoichiometric phase, $YbS_{1.33}$–$YbS_{\sim 1.46}$ with its own structure type: that of Yb_3S_4 (*4*), for which a subsequent electron diffraction study (*6*) revealed that nonstoichiometric $Yb_{3-\delta}S_4$ was modulated in the **b** direction, usually, but not always, incommensurately. The modulation period was ~7 × to ~8 × **b**. (iii) A nonstoichiometric phase $Yb_{1-\delta}S$ with the B1 (*NaCl*) structure; sometimes with doubled lattice parameter $a = 2 \times a$(B1). Later studies, especially of the analogous system CaS + Yb_2S_3 (*7*), indicated that there could be a small rhombohedral distortion of the larger cell at higher values of δ.

Most of these and other results have been comprehensively reviewed by Flahaut (*8*).

Note that in all the above structures the array of sulfur atoms appears to be complete and intact: nonstoichiometry is accommodated by omitting some cations from available sites, which are completely occupied in the stoichiometric compound.

Except for some minor discrepancies in stoichiometry, the results of Eliseev *et al.* (*9*) appear to be in broad agreement with those of Flahaut *et al.* But they also report some new phases and polymorphs at higher sulfur pressures (above several kilobars) at high temperatures. These additional results are not relevant to our 1-atm studies.

* To whom correspondence should be addressed. Permanent address, Research School of Chemistry, Australian National University, G.P.O. Box 4, Camberra, A.C.T. 2601, Australia.

0022-4596/90 $3.00

Here we give a further report (cf. (*6*)) on our, mainly electron diffraction, studies of Yb + S.

Experimental Methods

Sample Preparation

A sample of $Yb_{3-\delta}S_4$, previously made by heating 4 *N* Yb_2O_3 (in an inductively heated graphite crucible) in a stream of 5% H_2S + 95% Ar for 1.5 hr at ~1500°C (*6*), was used to prepare two new samples:

A, by heating in the same way, but now to ~1850°C for ½ hr, after which it was allowed to cool freely (in H_2S + Ar) to room temperature. The product had partly melted.

B, by arc-melting a pellet of the starting material for 1 min. The (unmeasured) temperature was probably 2000°C or more.

C, a third sample, was prepared–again by induction heating in a graphite crucible in a stream of 5% H_2S/Ar–but now using 4 *N* Yb metal and a temperature of ~1200°C for 2 hr. It was then allowed to cool freely to room temperature.

Diffraction Studies

The three samples were examined by X-ray powder diffraction, using a Guinier–Hägg focusing camera and monochromatic Cu $K\alpha_1$ radiation with 6 *N* Si as an internal standard, and also by electron microscopy/diffraction. For the latter, the sample was ground under ethanol, dispersed on Cu grids coated with holey-carbon support films, and examined in a JEOL 2000 FX or JEOL 200 CX microscope, both fitted with goniometer stages.

Experimental Results and Their Interpretation

The X-ray powder patterns were complex, with many lines (up to 79) observed in the range $5° < 2\theta < 90°$, suggesting the probable presence of several phases in each case. This was confirmed and clarified by electron diffraction, and the interpretation of these latter (single crystal) patterns necessarily preceded the resolution of the X-ray patterns which, it transpired, had many overlapping lines, especially for sample B, the X-ray pattern of which could not, finally, be unambiguously indexed.

X-ray Diffraction

Sample A. Of the 79 observed and measured diffraction lines 76 could be indexed on the basis of the orthorhombic (*Pnma*) unit cell of "Yb_3S_4;" the remaining 3 were of weak intensity. But 39 lines could also be indexed on a rhombohedral cell (with $a_r \approx \sqrt{2} \times a(B1)$), including one which did not fit the orthorhombic cell. Fourteen lines also fitted a cubic cell with $a_c = 2 \times a(B1)$, and three of these did not fit the orthorhombic cell.

Sample C. In this case the rhombohedral structure was not observed: the presence of (modulated) orthorhombic $Yb_{3-\delta}S_4$ is unequivocal. There also seems to be a cubic phase (with $a_c = a(B1)$).

It must be emphasized that determination of the phases present by analysis of the X-ray powder patterns was quite impossible (overlapping lines), and their identification is not made in this way. This comes from the electron diffraction patterns (see below), some of which are also ambiguous. The X-ray data (with the exception of sample B) simply enable unit cell parameters to be refined—once the approximate unit cell size has been determined by elecron diffraction. Unit cell parameters thus deduced are listed in Table I.

Electron Diffraction

Seven different sorts of structures (1*a* and *b*, 2, 3*a* and *b*, and 4*a* and *b*) were identified by this means but they derive from only

TABLE I

REFINED UNIT CELL PARAMETERS FROM X-RAY DIFFRACTION DATA

(i) Orthorhombic ($Yb_{3-\delta}S_4$) structure

Sample	a/Å	b/Å	c/Å	V/Å^3	v(S)/Å^3*
A	12.777(3)	3.837(1)	12.926(2)	633.7(2)	39.61
C	12.628(5)	3.804(2)	12.817(4)	615.7(4)	38.48

(ii) Rhombohedral structure

Sample	a_r/Å	α_r	a_h/Å	c_h/Å	$V_h = 3V_r$/Å^3	v(S)/Å^3*	c_h/a_h†
A	8.012	59.08°	7.901(3)	19.76(1)	1068.3(7)	44.5_1	2.50_1
B	8.111	58.77°	7.959(3)	20.05(2)	1099.7(9)	45.8_2	2.51_9

(iii) Cubic structures

Sample	a/Å	V/Å^3	v(S)/Å^3*
A	11.271(2)	1431.7(9)	44.7_4
B	11.151(2)	1386.6(8)	44.3_3
C	5.647(3)	180.1(3)	45.0_2

* v(S) equals volume per S atom.

† c/a for equivalent hexagonal unit cell.

four (or perhaps even three) basic structure types. These are:

(1) The *orthorhombic, Pnma,* Yb_3S_4 type, which occurs as two variants:

(*a*) modulated—the diffraction patterns exhibiting weak but sharp satellite reflections (incommensurate with respect to the reciprocal lattice net of Bragg reflections);

(*b*) unmodulated—with diffraction patterns consisting only of the Bragg reflections characteristic of the orthorhombic subcell.

(2) The *orthorhombic, Cmcm,* $CaTi_2O_4$ type, which has not previously been reported for Yb_3S_4 (in the binary system). However, it has been reported (*10*) as the high temperature form of $CaLn_2S_4$ (*Ln* = Ho to Lu and Y)—the low temperature polymorph again being (except for Ho) the *Pnma,* Yb_3S_4 structure. (It was also stated that this high-temperature form also had a homogeneity range, and that transformation *Pnma* → *Cmcm* is reversible, but sluggish (*10*).)

If the unit cell axes of the *Cmcm* structure are interchanged to correspond with those in the *Pnma* form, the new setting ($\bar{\mathbf{b}}$ **a c**) is *Ccmm*. The polymorphs can then be distinguished by their different extinction conditions. (Their unit cell axes are of very similar lengths ~12 × 4 × 12 Å.)

	Pnma	*Ccmm*
h k l	No conditions	$h + k = 2n$
h k 0	$h = 2n$	$h + k = 2n$
0 *k l*	$k + l = 2n$	$k,l = 2n$
h 0 *l*	No conditions	$h = 2n$

(3*a*) The *cubic, Fm*3*m,* B1 (= NaCl) structure type reported for "YbS", with minimum deficiency of Yb, i.e., $Yb_{1-\delta}S$ with a small value of δ.

(3*b*) The related *cubic* structure with a doubled unit cell axis, $a = 2 \times a$(B1), reported for larger values of δ.

Finally,

(4) The slight *rhombohedral* distortion of this "doubled B1" cell sometimes observed for even larger values of δ. It has not previously been seen for $Yb_{1-\delta}S$ (*2, 11*), but has been observed in related systems, e.g.,

TABLE II

DIFFERENT PHASES (TYPES OF ELECTRON DIFFRACTION PATTERN) OBSERVED IN THE VARIOUS YbS_x PREPARATIONS

	Phase: Orthorhombic			(3) Cubic		(4) Rhombohedral	
	(1) *Pnma*		(2) *Ccmm*				
Sample	*a* (+ satellites)	*b* (no satellites)	(no satellites)	*a* = *a*(B1)	*b* = 2*a*(B1)	*a* (+ satellites)	*b* (no satellites)
A	N[a]	Y[a]	N	N	Y	Y	Y
B	N	Y	Y	N	Y	N	Y
C	Y	N	N	Y	?	N	N

[a] N, nonobserved; Y, observed.

the ternary (pseudobinary) analogue CaS + Yb_2S_3 (*2*).

By analogy with the behavior of $Yb_{1-\delta}Se$ (*12*), Tomas *et al.* (*11*) have suggested that their sample of $Yb_{0.875}S$ ($\delta = 0.125$), which they studied by single crystal X-ray diffraction, was probably rhombohedral even though they could index the reflections on a doubled cubic unit cell and deduced the space group $F\bar{4}3m$. Their suggestion (following Hodges *et al.* (*13*), who studied $Tm_{0.79}Se$) was that the unique [111] axes of small rhombohedral domains were randomly oriented in all four ⟨111⟩ directions of a parent cubic structure. They also searched for weak satellite reflections and diffuse scattering, but found neither.

On the other hand, we have observed distinctly rhombohedral structures, electron diffraction patterns from which *a* sometimes contain weak satellite reflections (in addition to much stronger Bragg reflections characteristic of the rhombohedral cell), but *b* sometimes do not.

Table II summarizes the distribution of the various structure types in the three different samples, and we now give examples of electron diffraction patterns for each case, and for each sample where they are observed.

(*1*) *The Pnma Structure of the Yb_3S_4 Type*

(*a*) *Modulated.* This is observed only in Sample C.[1] Figure 1a is a $[001]_{Pnma}$ zone axis pattern with satellites at $\Delta \sim 6.3$. Other measured values were $5.7_2 \leq \Delta \leq 7.6_0$; i.e., somewhat lower than previously observed (*6*).

Figure 1b is a more complex pattern: it is simply indexed as a composite of two zone axis patterns, $[101]_{Pnma}$ and $[102]_{Pnma}$. Clearly the crystal is tilted so that both these zones are excited simultaneously.[2] In this case $\Delta \sim 7.3$.

(*b*) *Unmodulated.* Diffraction patterns with Bragg reflections due to the *Pnma* cell, but without satellites, are observed for samples A (Fig. 2) and B (Fig. 3) but not C.

[1] Sample A, after reheating in H_2S + Ar at lower temperatures, was the subject of earlier papers (*6*). Many electron diffraction patterns from it contained primary ("e_1") satellites at $(h, k + \frac{1}{2} \pm 1/\Delta, 0)$ with $h = 2n + 1$ and Δ in the range 6.9_2 to 8.5_0 in various crystals. Higher order satellites were also present. In one (commensurate) case $\Delta = 8$ exactly. Not all diffraction patterns contain satellites.

[2] Note the slight nonorthogonality of the principal rows of reflections (~89° instead of 90°). The angle between these zone axes is 18.3°: a tilt error of ~9° from each zone axis can account for this ~1° error.

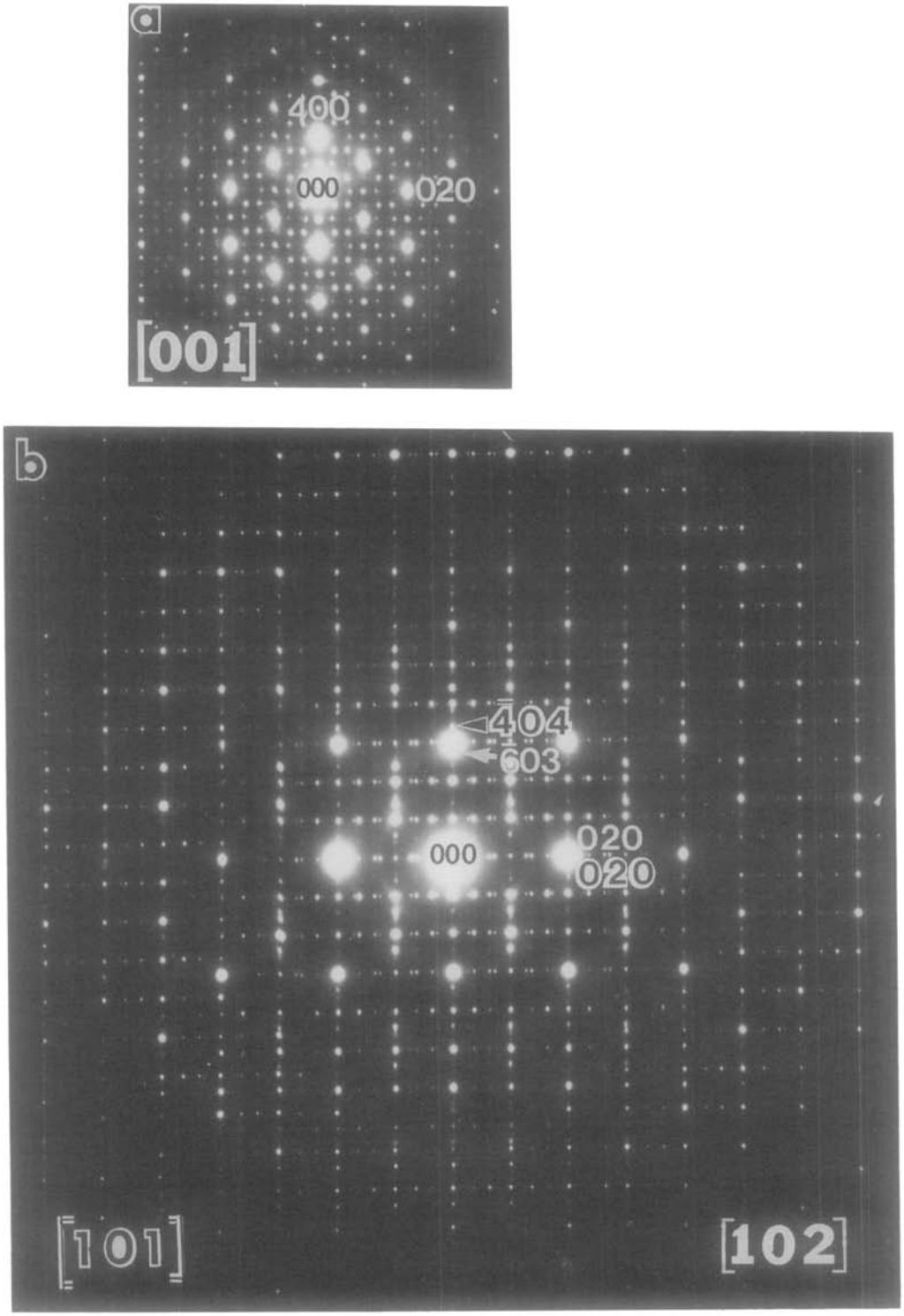

FIG. 1. (a) Electron diffraction pattern from a modulated, Yb_3S_4 type, crystal of sample C; incident beam parallel to $[001]_{Pnma}$. The satellite reflections along **b*** correspond to $\Delta \sim 6.3$ ($\lambda_b \sim 24$ Å). (b) Complex electron diffraction pattern from another modulated, Yb_3S_4 type, crystal of sample C. It can be indexed as a composite of two zone axis patterns $[101]_{Pnma}$ and $[102]_{Pnma}$, as indicated. Here $\Delta \sim 7.3$.

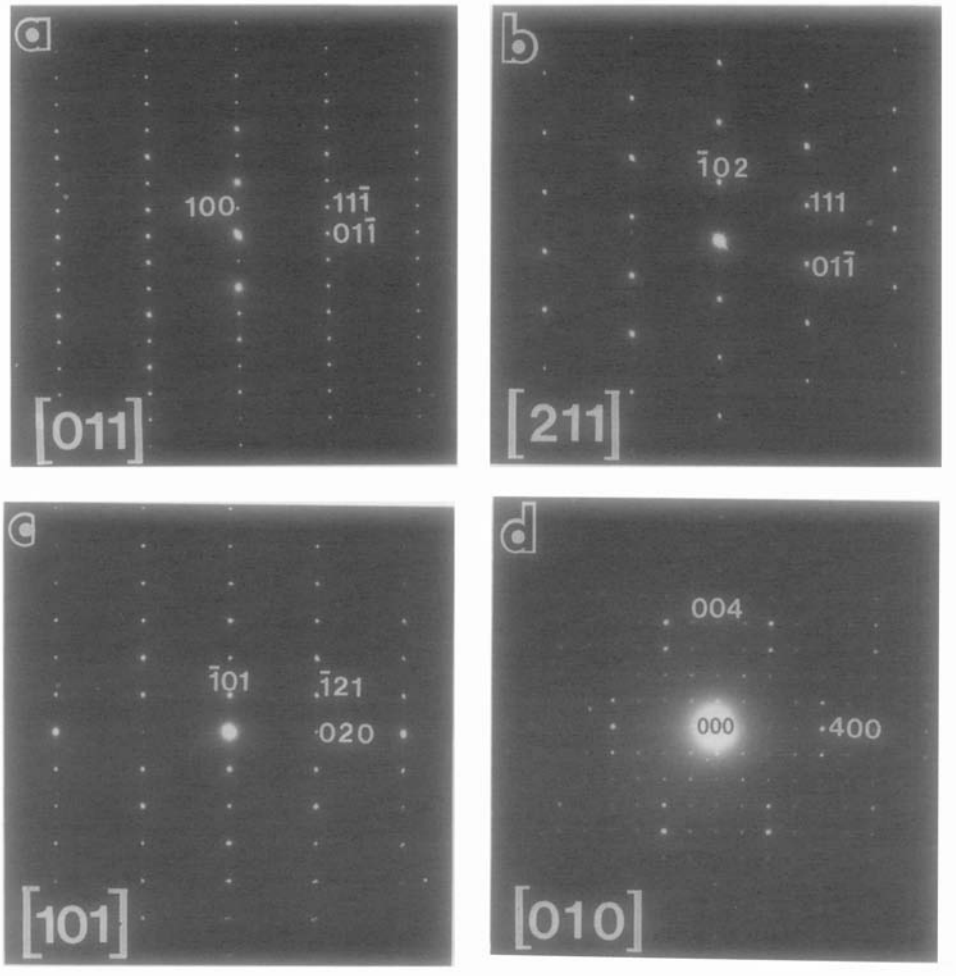

FIG. 2. (a–d) Set of diffraction patterns from two different crystals of sample A corresponding to unmodulated orthorhombic *Pnma* Yb_3S_4 type. Note the absence of satellite reflections. Zone axes are indicated. (e) High resolution image from a well-ordered crystal flake of sample A taken with the incident beam parallel to [001] of the *Pnma*, Yb_3S_4 phase; the inset (f) is the corresponding diffraction pattern.

Diffraction patterns occasionally showed very weak streaking in the $\mathbf{c}^*$ direction, with corresponding fault planes parallel to $(001)_{Pnma}$ in the image. This has not yet been explored.

(2) *The Ccmm Structure of the* $CaTi_2O_4$ *Type*

Diffraction patterns corresponding to this structure were observed only from the highest temperature preparation, sample B: one is shown in Fig. 4. Although the *d* spacing must be very similar in the *Pnma* and *Ccmm* structures, this figure cannot be indexed as *Pnma*: in particular, for *h*0*l* reflections there are no conditions in *Pnma* (Fig. 2d) but, for *Ccmm*, $h = 2n$ (Fig. 4).

This is the first observation of this structure in the binary system; i.e., it is a new polymorph of "Yb_3S_4."

Another crystal fragment was clearly

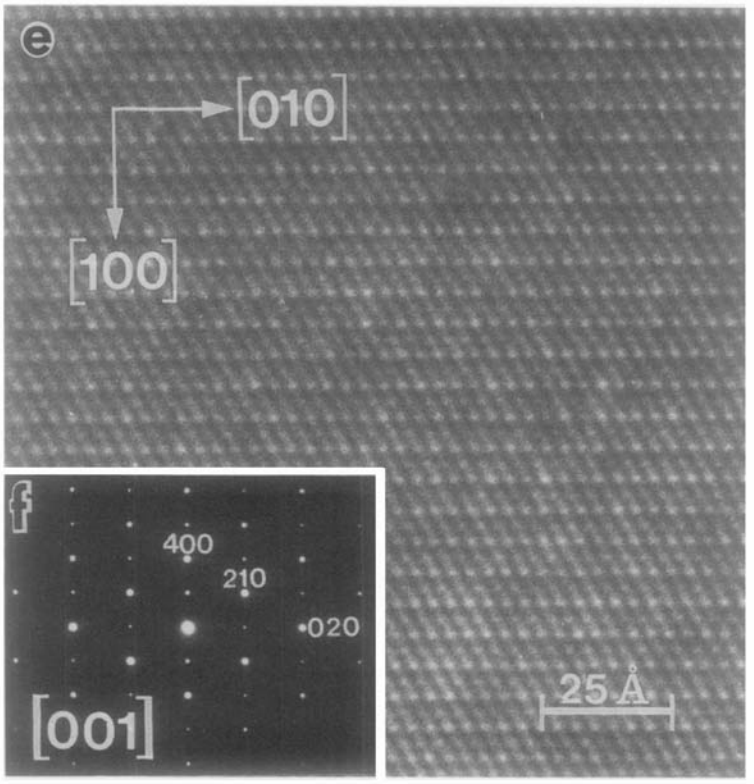

FIG. 2—*Continued*

Pnma in one part, but *Ccmm* in another (Fig. 5).[3]

The *Ccmm* structure was by no means always perfect, Fig. 6, but the nature of the faults has yet to be determined.

(3) *The Rhombohedral Structure of* $Yb_{1-\delta}S$

(*a*) *Modulated.* In our earlier paper (*6*), we pointed out that three different phases could be identified in "high temperature" preparations of YbS_x. One of these gave electron diffractions patterns with Bragg reflections superficially similar to $[001]_{Pnma}$ zone axis patterns from "Yb_3S_4," but with alternate allowed "h00" reflections absent. In addition there was a complex, two-dimensional array of weak satellite reflections, quite different from that from "Yb_3S_4" (e.g., Fig. 7 of Ref. (*6*)). The array of satellites suggested a two-dimensional modulation, possibly commensurate with "910^*_{Pnma}"—with a multiplicity of 13 × $d(910)_{Pnma} \sim 16.0$ Å.

Identical patterns are frequently observed from sample A: Fig. 7 is an example. Note that the *thin* part of the crystal, and its corresponding diffraction pattern (compare Fig. 2f) do not reveal the modulation—a common observation for both modulated- and superstructures.

Figure 8 is from another crystal: it shows far fewer satellites than Fig. 7, although the

[3] These two structures may be simply related by slip on (100) planes, as has been discussed elsewhere (*14*).

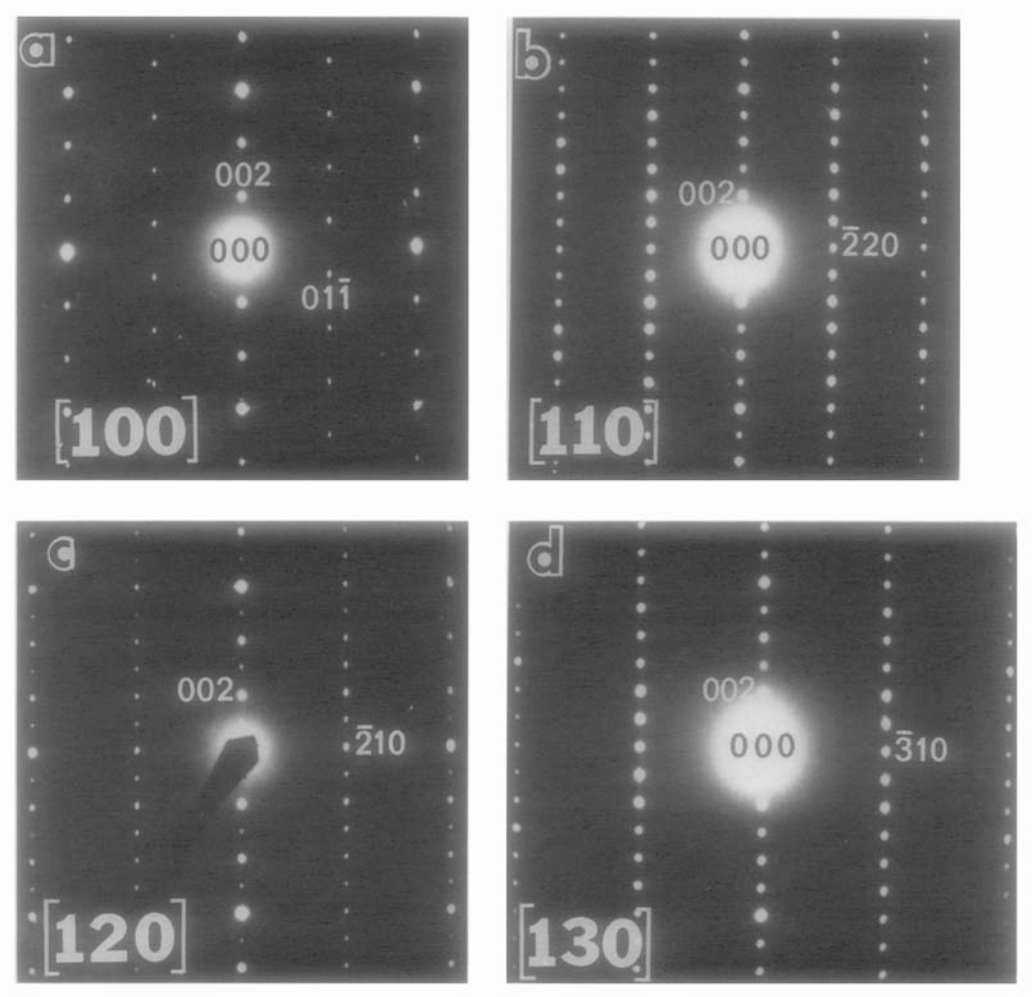

FIG. 3. (a–d) Series of electron diffraction patterns from an unmodulated, Yb_3S_4 type, crystal of sample B. Zone axes are $[1v0]_{Pnma}$, with $v = 0, 1, 2, 3$.

pattern of Bragg reflections appears to be the same in both cases: $[\bar{1}10]_h \equiv [\bar{1}2\bar{1}]_r$ zone axis,[4] equivalent to the pseudocubic $[1\bar{2}1]_h$. Since the rhombohedral unit cell (with $a_r = 8.012$ Å $\sim \sqrt{2} \times a_c$, $\alpha_r = 59.08°$; Table I) is only a small distortion of the pseudocubic subcell there are many (12) "pseudoequivalent" zone axes, only two of which ($[\bar{1}\bar{1}2]_r$ and $[2\bar{1}\bar{1}]_r$) are truly $\equiv [1\bar{2}1]_c$. It is presumably one of these latter which is obtained in Fig. 8: equivalent in terms of Bragg reflections, but not in its pattern of satellite reflections.

(*b*) *Unmodulated.* The immediately preceding discussion suggests the possibility that the absence of satellites from a diffraction pattern (from the rhombohedral phase) may be due to an inappropriate zone axis (or a very thin crystal!). We believe the following cases are not vitiated in this way.

The unmodulated rhombohedral struc-

[4] Subscripts *h*, *r*, and *c* indicate (equivalent) hexagonal, rhombohedral, and (pseudo-)cubic unit cells.

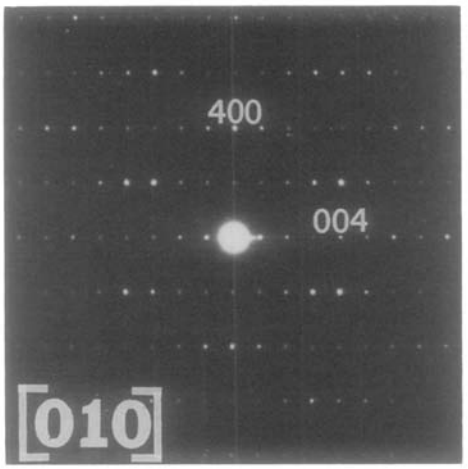

FIG. 4. Electron diffraction pattern from a crystal of sample B corresponding to [010] zone axis of the *Ccmm* Yb_3S_4 structure.

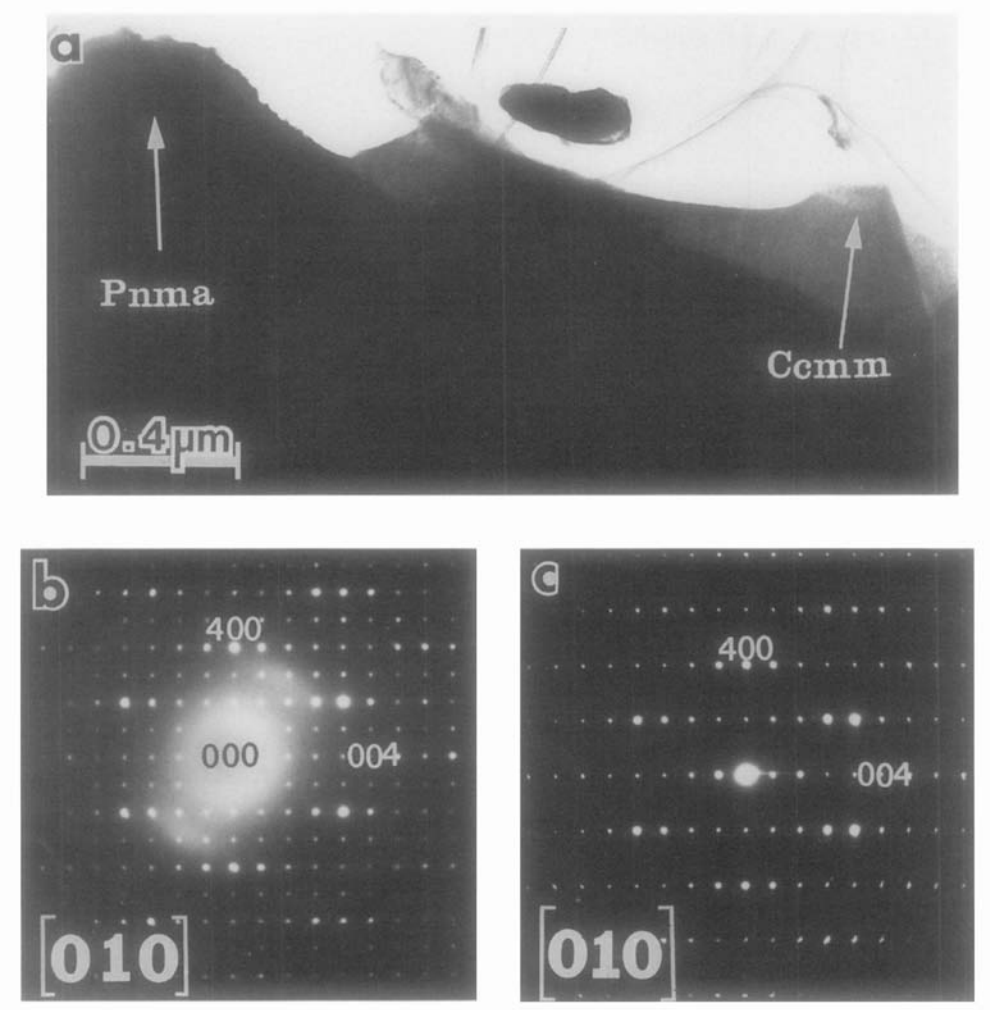

FIG. 5. (a) Low magnification image from a crystal of sample B. Diffraction patterns from different areas of the crystals, which have been indicated. (b) Zone axis $[010]_{Pnma}$. (c) Zone axis $[010]_{Ccmm}$.

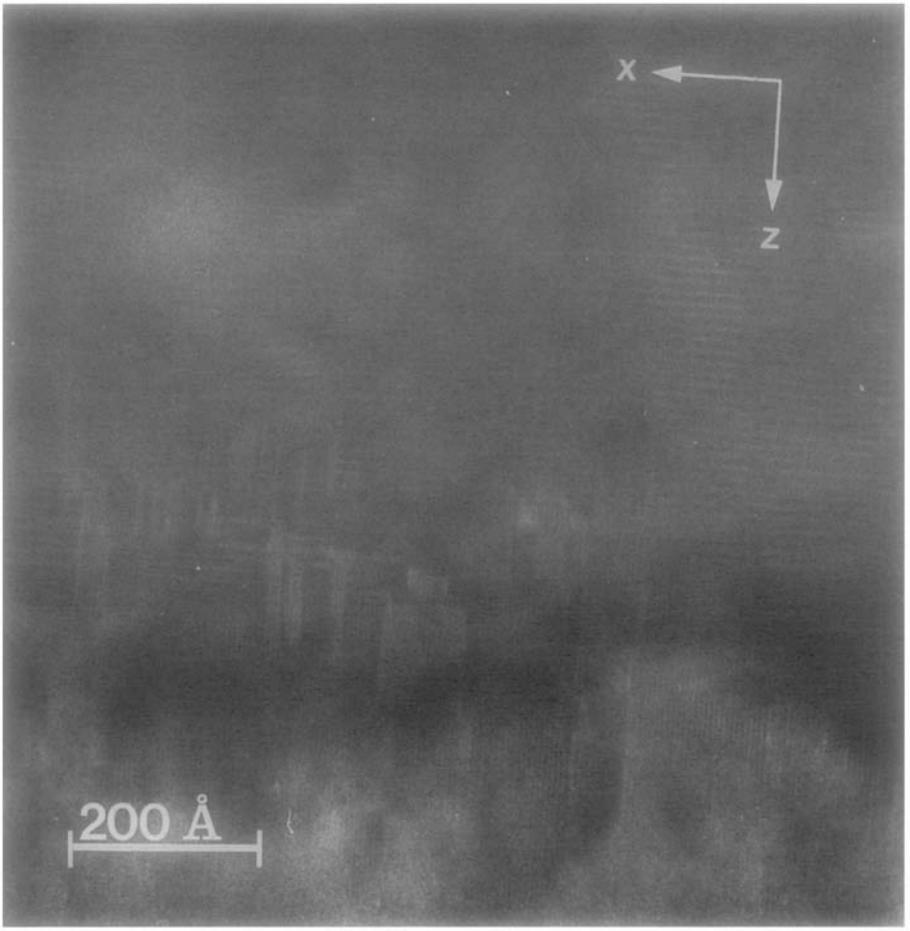

FIG. 6. Enlarged magnification micrograph of the *Ccmm* phase with the incident beam parallel to $[010]_{Ccmm}$. Fringes corresponding to (001) planes ~12 Å and (200) ~6 Å are visible.

ture is observed in samples A and B. An example from A is shown in Fig. 9a and from sample B in Figs. 10a and 10c. Both images, Figs. 9b and 10b suggest some disorder, especially the latter. While it is not possible to interpret this unequivocally, it appears to be consistent with twinning ($[111]_r$ parallel to various $\langle 111 \rangle_c$), cf. the narrow lattice fringes and wide moiré fringes, as suggested by Tomas *et al.* (*11*).

Figure 11a is an even more complicated image of rhombohedral phase material from sample B. At first sight, the corresponding diffraction pattern (Fig. 11b) looks very complex, and lacking in symmetry; but it is readily indexed as arising from two overlapping crystals with a common zone axis, $[1\bar{1}0]_h$, one being rotated by ~17° with respect to the other. Figure 11c shows part of the diffraction pattern indexed in this way: strong double diffraction is responsible for the many extra reflections, including the very obvious hexagon of spots around each Bragg reflection. The six vectors between each Bragg reflection and the vertices of its surrounding hexagon are 113* − *113**,

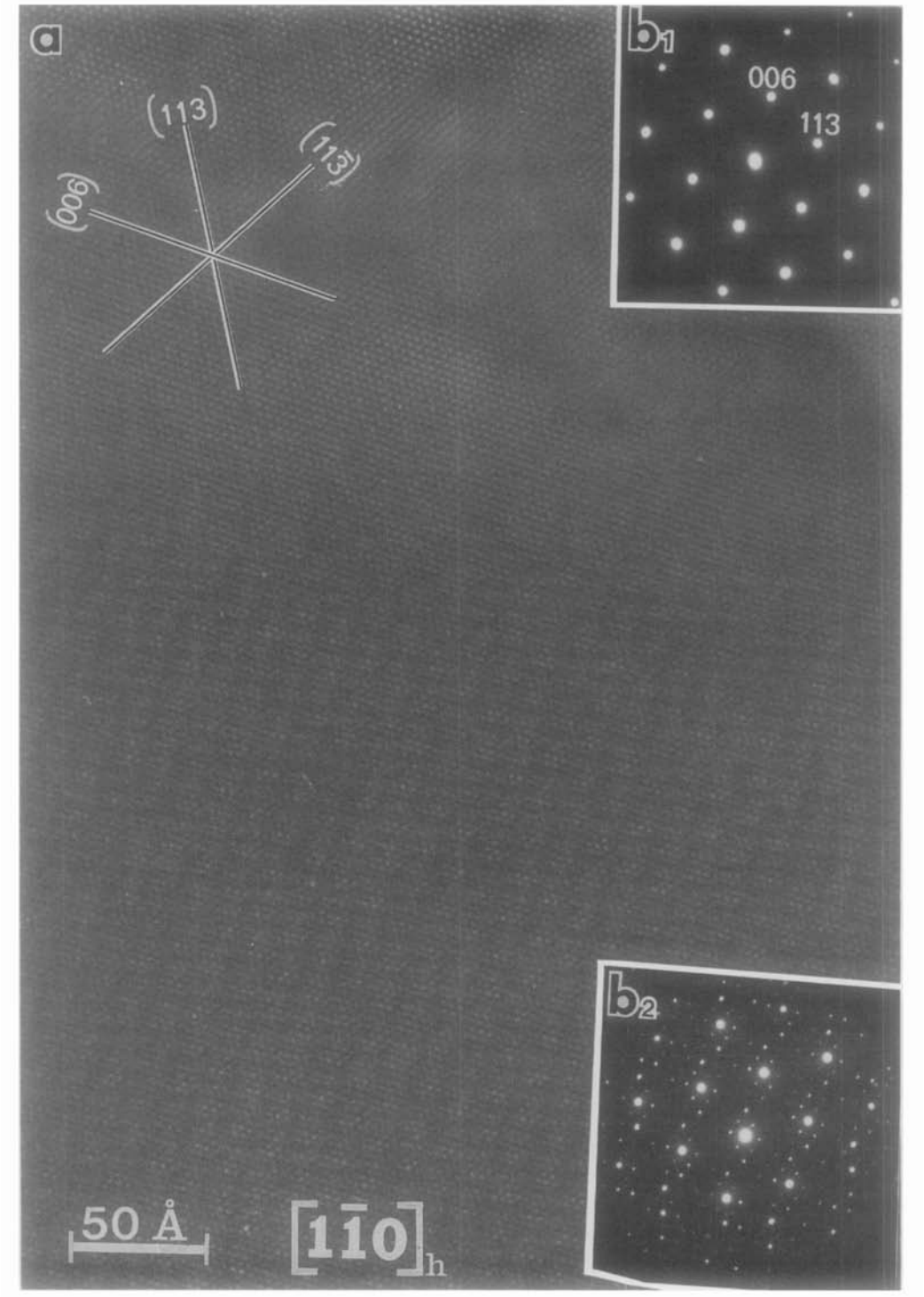

FIG. 7. Image from a crystal of the rhombohedral phase, sample *A*: zone axis $[1\bar{1}0]_h \equiv [\bar{1}2\bar{1}]_r$. Inset are the selected area diffraction patterns from the thinner (top) and thicker (bottom) parts of the crystal. Note the apparent absence of the two-dimensional modulation in the former.

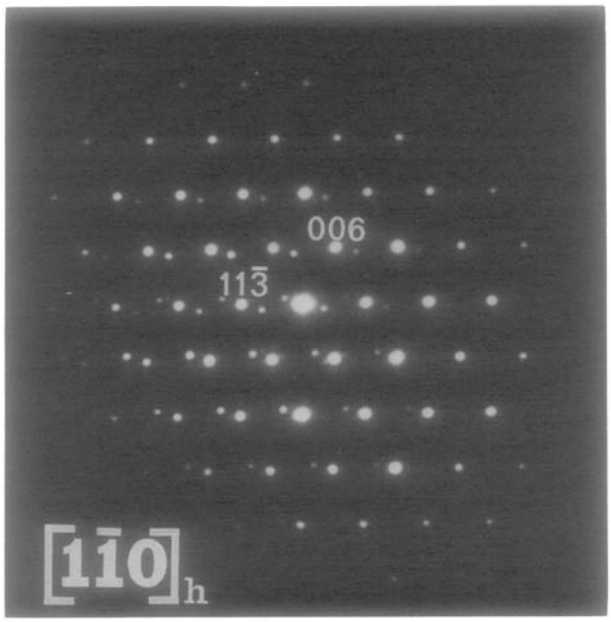

FIG. 8. Electron diffraction pattern from a crystal of sample A along $[\bar{1}10]_h$ of the rhombohedral phase. Note the different shape and position of the satellite reflections compared with those in Fig. 7.

$11\bar{3}^* - 11\bar{3}^*$, and $006^* - 006^*$. Apart from their common zone axis the relative orientations of the two crystals appears to be arbitrary: we could detect no evidence of a small (real space) coincidence cell. The shortest reciprocal spacings in Fig. 11b (11c) give rise to the moiré fringes (indicated by arrowheads) in Fig. 11a.

The corresponding zone axis pattern (and image) for a single crystal in this orientation is shown in Fig. 12.

3. *Cubic Structures (Also Related to B1 Type)*

(*a*) *Superstructure with* $a_c = 2 \times a(B1) \approx 11.3$ *Å*. The relative precision with which one can measure similar reciprocal lattice vectors on an electron diffraction pattern (even excluding variations in camera constant) is sometimes barely sufficient to allow one to distinguish this superstructure of B1 from its rhombohedrally distorted variant discussed above. But the intensity differences between "cubically equivalent" reflections (e.g., $111^*_c + \bar{1}11^*_c$) help: compare, for example, Fig. 10c (rhombohedral, from sample B) with Fig. 13d, a similar zone axis pattern from sample A. The later may be cubic ($\bar{1}1\bar{1}^*_c \approx 111^*_c$ in intensity), but the former cannot be ($101^*_h \equiv \bar{1}1\bar{1}^*_c \neq 111^*_c \equiv 003^*_h$). But, of course, it is always possible that the former 111^*_c is actually, say 011^*_h: a different hexagonal zone axis of a rhombohedral structure (that is equivalent in a cubic strucure). Figure 13 is a group of diffraction patterns from one crystal of sample A indexed as cubic, with $a_c = 2 \times a(B1)$.

A group of diffraction patterns from another crystal of sample A is shown in Fig. 14, together with the image corresponding to one of them. Again, cubic or rhombohedral indexing is possible (with a "double (pseudo-?) cubic cell"). But the image shows great heterogeneity, either in orientation (of small, 50–80 Å, domains) and/or lattice parameter: notice the basic fringes plus moiré fringes.

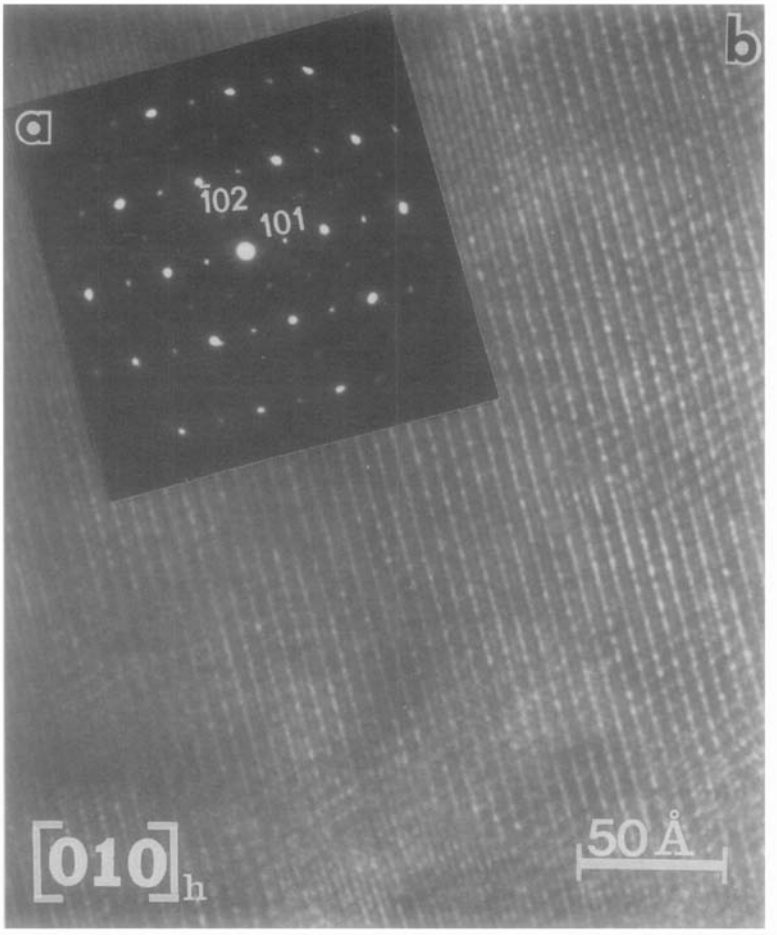

FIG. 9. (a) Electron diffraction from a crystal of sample A. Incident beam is parallel to $[010]_h$. Note the absence of satellite reflections in this orientation. (b) Micrograph of the same crystal showing subcell and moiré fringes.

Clearly, the electron diffraction technique is not able to resolve the relevant questions in this area (of cubic structures), and we recall that Tomas *et al.* (*11*) appear to have a similar difficulty; in that case with single crystal X-ray diffraction!

Discussion

Qualifications

Except for the rhombohedral phases, we are not confident about interpreting our results on the cubic or pseudocubic, B1-related structures, particularly for sample B. This is true for electron diffraction patterns (possible lens aberrations, difficulty in ensuring exact orientation) and for the X-ray powder diffraction patterns (multiphase, with many lines—a number of which overlap). Here, therefore, we concentrate on the other structures.

Unit Cell Volumes

With the possible exception of Eliseev (*9*), it seems to be generally agreed that all the sulfides with which we are here con-

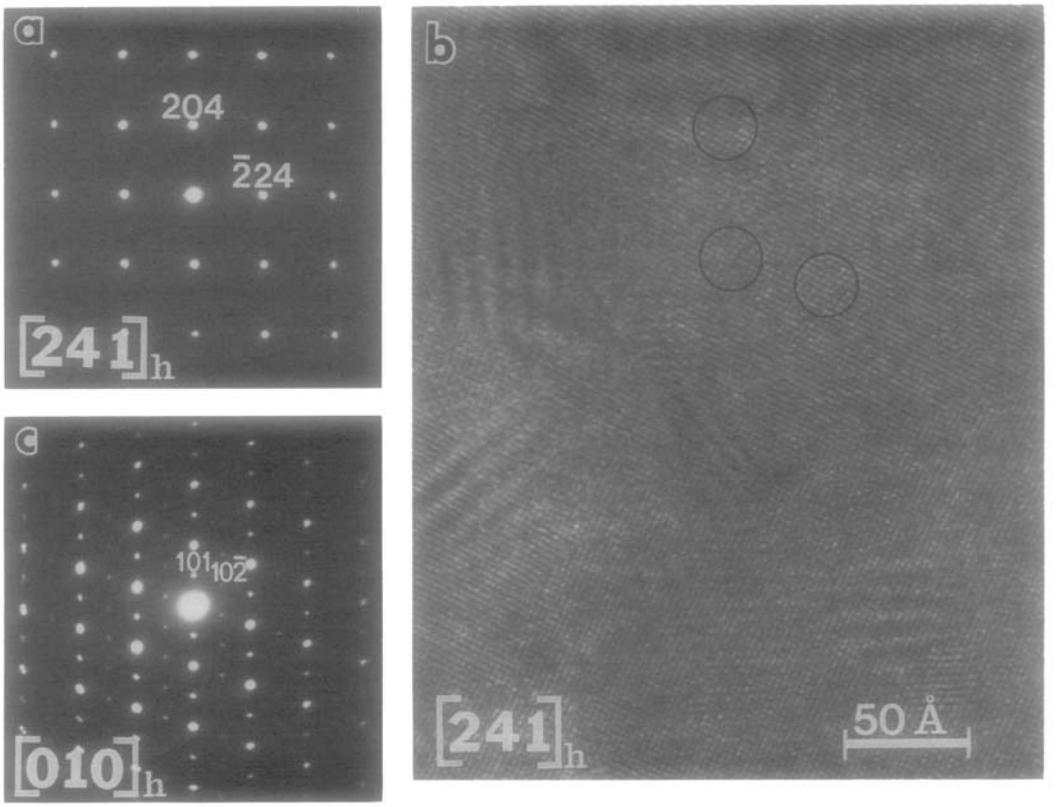

FIG. 10. (a,b) Electron diffraction patterns from two different crystals of sample B, see text for explanation. (c) Lattice image corresponding to the crystal giving the diffraction pattern shown in (a).

cerned have complete anion arrays ("lattices"), although the cation arrays are frequently incomplete. On the basis of this assumption we have, where possible, calculated (from the X-ray-derived data in Table I) the volume per sulfur atom for each observed structure. These volumes are indicated by arrows in the lower part of Fig. 15, which shows the relation between the stoichiometry (x in YbS_x) and volume per sulfur atom, as determined from several sources: (i) Patrie *et al.* (*7*) for the cubic/rhombohedral phases (of CaS + Yb_2S_3, rather than the binary YbS_x); (ii) the data of Eliseev *et al.* (*9*) for the same phases in the binary system (uncorrected, and also

FIG. 11. (a) Micrograph of a crystal of the rhombohedral phase in sample B; incident beam parallel to $[\bar{1}10]_h$. (b) Electron diffraction pattern corresponding to Fig. 11a. (c) Interpretation of Fig. 11b: Bragg reflections of two differently oriented crystals are indicated by the larger circles, and some of the double diffraction spots by smaller ones. The principle double diffraction vectors are indicated by the arrowed full lines and broken lines. (Each of the second set is, of course, a combination of two from the first set.) These give rise to a group of reflections around each Bragg spot as indicated around the origin. Each of these doubly diffracted reflections can also be the center of a similar group and, in this way, all reflections are accounted for. The two "unit cells" are also shown, and some Bragg reflections are indexed. (Indices for the second crystal are underlined.)

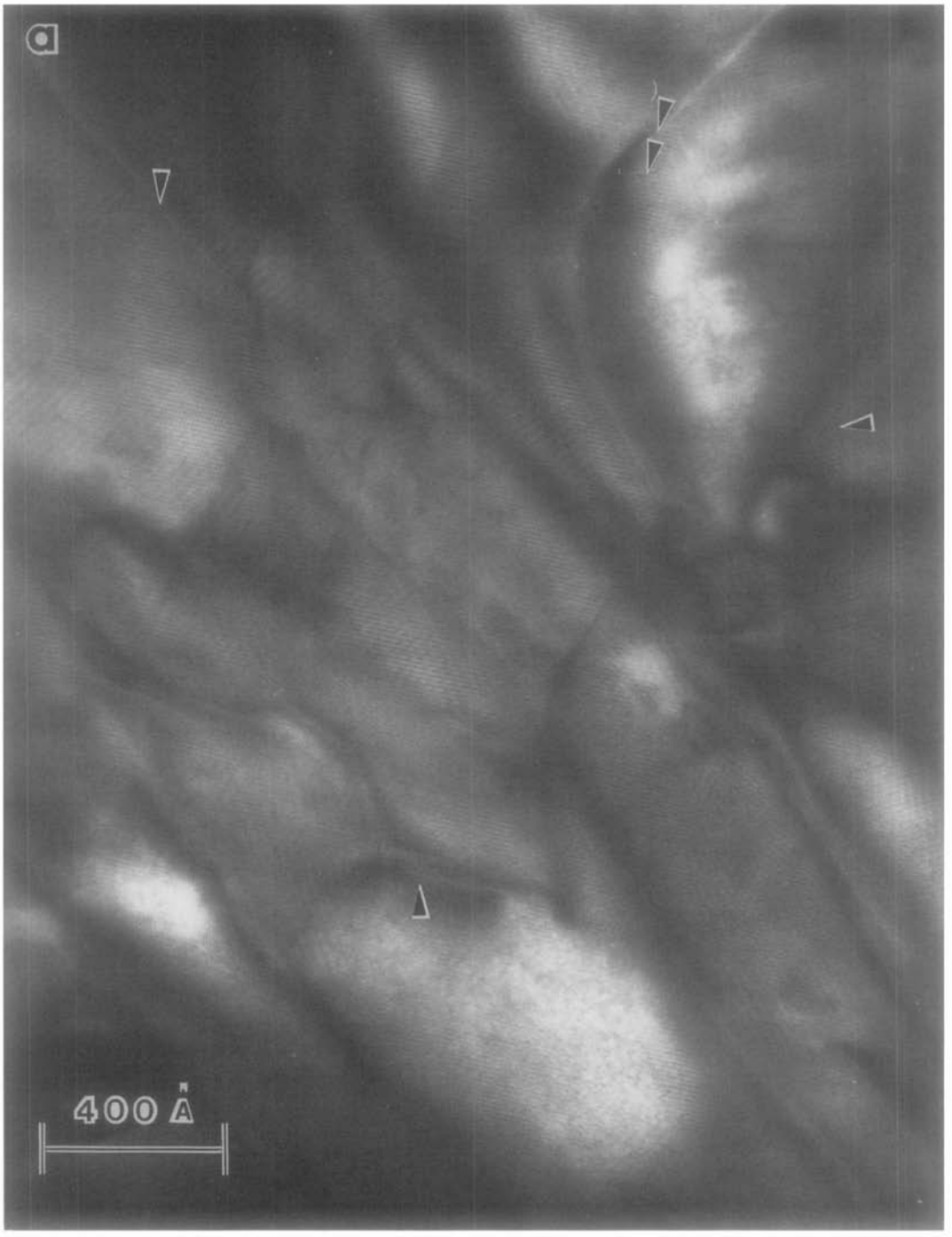
a
400 Å

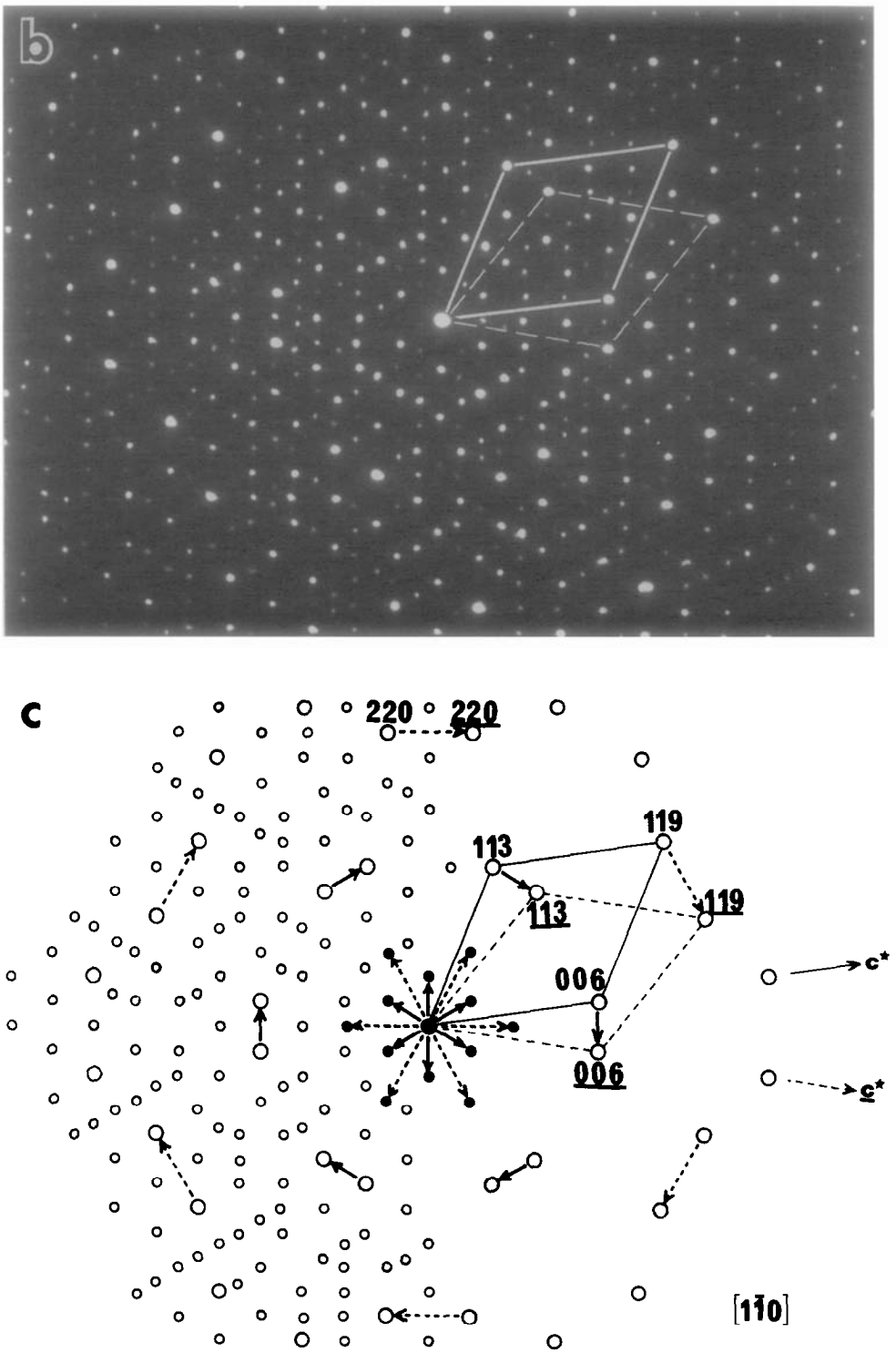

FIG. 11—*Continued*

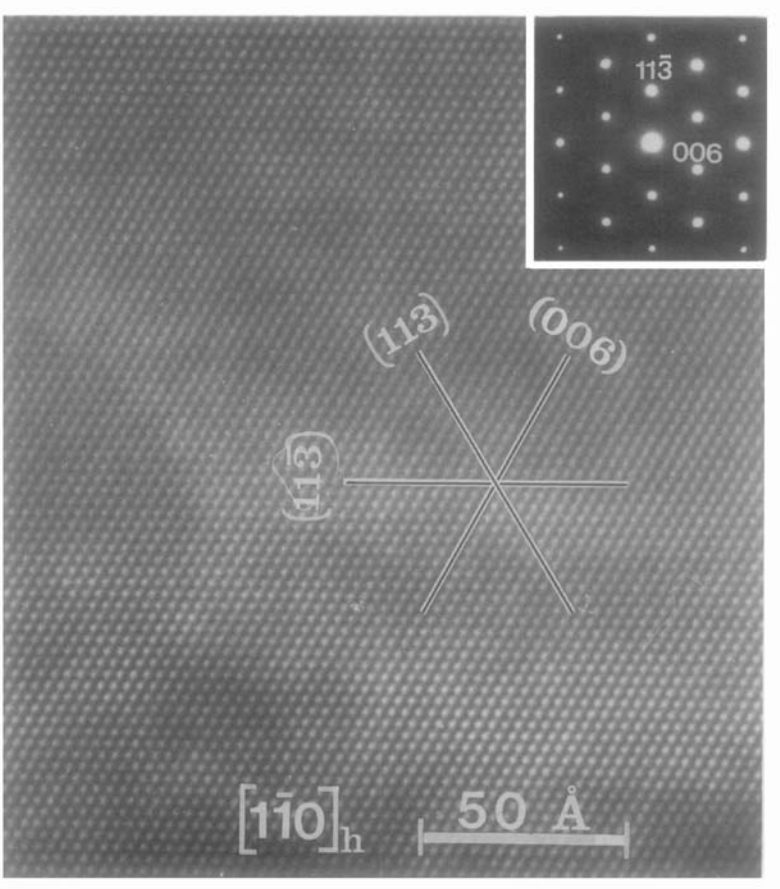

FIG. 12. High-resolution micrograph corresponding to the basic rhombohedral phase $Yb_{1-\delta}S$ along $[\bar{1}10]_h$ and its corresponding diffraction pattern. (These come from a different area of what appears to be the same "crystal" that yielded Fig. 11.)

corrected for what we believe to be their underestimation of x—based on our experience in electron microprobe analysis and also the assumption that nonstoichiometry arises only from a cation deficiency, the anion array being intact); and (iii) an extension of Fig. 2 in our earlier paper (*6*) for the *Pnma*, "Yb_3S_4" structure.[5]

This figure shows a number of things:

(i) That the "Yb_3S_4" structure is very compact, compared even with the corundum type of Yb_2S_3 at the same stoichiometry (when the former has a proportion of empty cation sites in the trigonal prisms), and especially with the B1 and related types.[6]

(ii) The point for Tomas *et al.*'s $Yb_{0.875}S$ falls right on our "corrected" line for Eliseev's data.

[5] There are 16 atoms in the *Pnma* (and *Ccmm*) unit cells of "Yb_3S_4"; 4 S atoms in the B1 f.c.c. unit cell, 32 S atoms in the "doubled B1 f.c.c." cell with $a_c = 2 \times a(B1)$, 8 S atoms in the derived rhombohedral cell of the latter with $a_r = \sqrt{2} \times a(B1)$, and hence 24 S atoms in the corresponding hexagonal unit cell.

[6] Note, in passing, that this is so even though corundum and B1 have "closed-packed" sulfur arrays while Yb_3S_4 does not: i.e., the "close-packed" arrays are less efficient than the one that is not "close-packed".

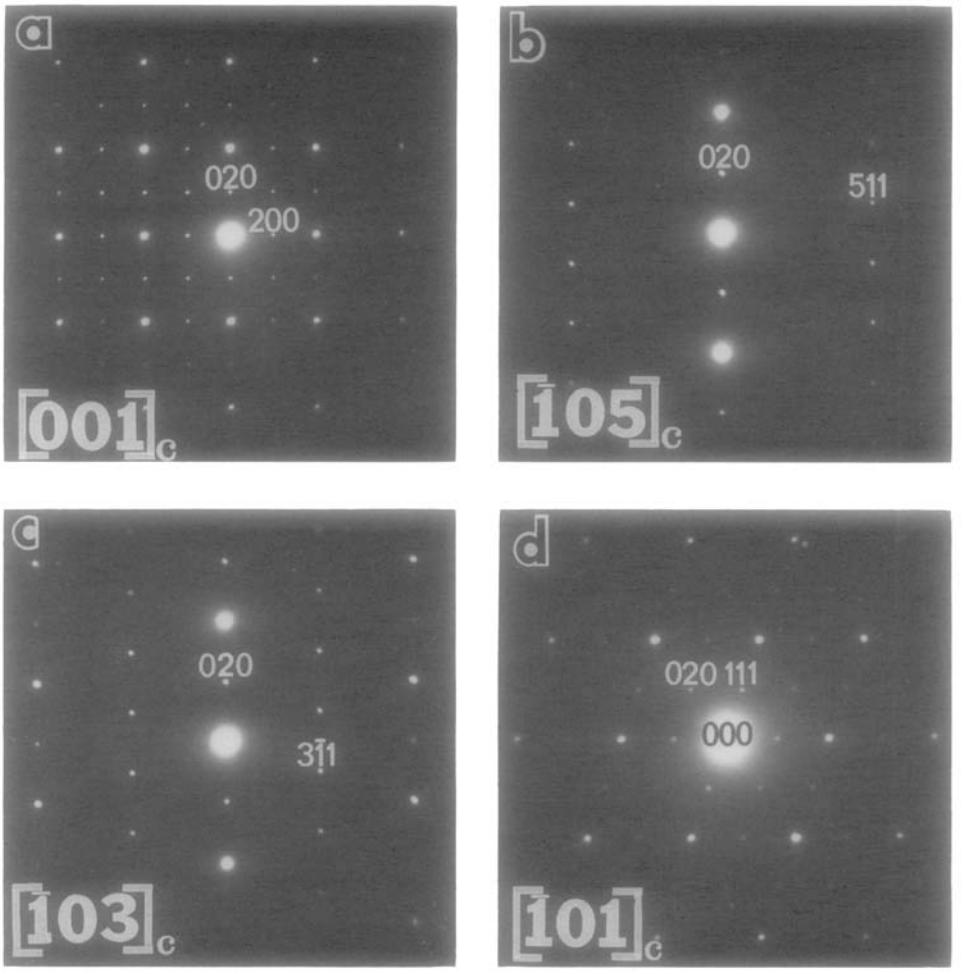

FIG. 13. Series of electron diffraction patterns taken from one crystal of sample A. The indexing refers to a unit cell with cubic symmetry and $\mathbf{a} = 2\mathbf{a}_0$.

(iii) Some of Flahaut *et al.*'s data (for $Yb_{3.0}S_4$ and corundum-type Yb_2S_3) appear to disagree slightly with our values.

(iv) The volumes for our various preparations (indicated by arrows).

This figure is useful in the following analysis.

Analysis of Results

On heating in 5% H_2S (in Ar) the relative activity of sulfur decreases as the temperature increases, so that x (in YbS_x) also decreases. Our observations, some of which are summarized in Fig. 16, are consistent with this.

"Yb_3S_4" phase. It is the most oxidized phase (highest x) observed in these experiments. Sometimes its diffraction patterns contain additional weak satellite reflections, and sometimes they do not; the conditions for the former are lower temperatures (and therefore higher values of x), sample C only; and for the latter, higher temperatures (and lower values of x), samples A and B.

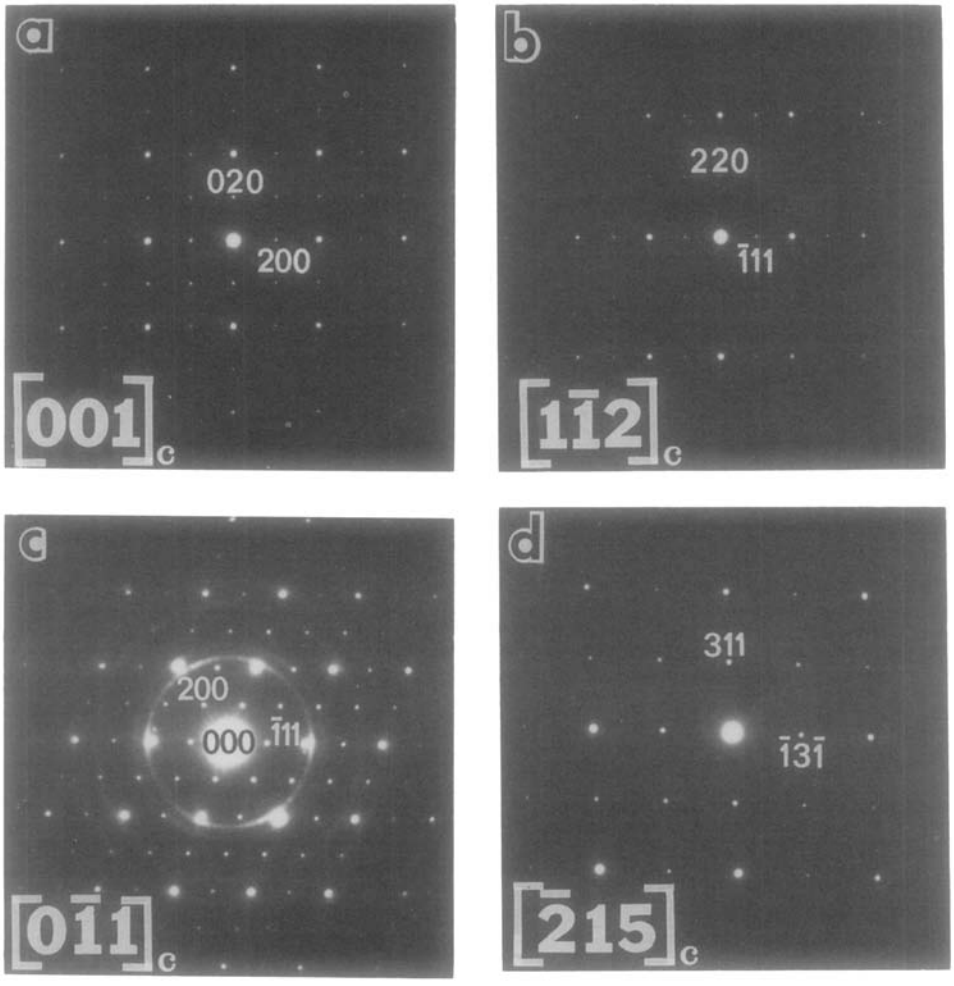

FIG. 14. (a–d) Series of electron diffraction patterns from a crystal of sample A. Zone axes and indices are for a cubic structure with $a = 2a_0$(B1) and a rhombohedral phase with $a_r = 2/\sqrt{2}\, a_0$. The micrograph corresponding to the $[001]_c$ orientation (Fig. 14a.) is shown in e.

The composition of this phase is said to range from $YbS_{1.33}$ ($= Yb_3S_4$) to $YbS_{1.48}$ (*8*) (just short of Yb_2S_3). At the former composition all the cation sites are occupied, $[Yb^{2+}](Yb^{3+})_2S_4$:[7] as the ratio S/Yb increases (the ratio Yb/S falls) a proportion of the trigonal prisms sites is vacated and some of the remaining Yb^{2+} are oxidized to Yb^{3+}; one then has, for $Yb_{3-\delta}S_4$, $[Yb^{2+}_{1-3\delta}Yb^{3+}_{2\delta}\square_\delta](Yb^{3+})_2S_4$. It seems likely (*6*) that the satellite reflections are basically due to a periodicity in the probable occupancy of the trigonal prism sites in the $\mathbf{b}_{Pnma}$ direction (in which the prisms share triangular faces to form rectilinear chains).[8] It follows that there can be no satellites at the stoichiometric composition, Yb_3S_4, with $\delta = 0$. We believe that this accounts for the absence of

[7] [ ] Indicates cations in trigonal prism sites; ( ) indicates cations in octahedral sites.

[8] Note that this periodicity does not, however, correspond to δ.

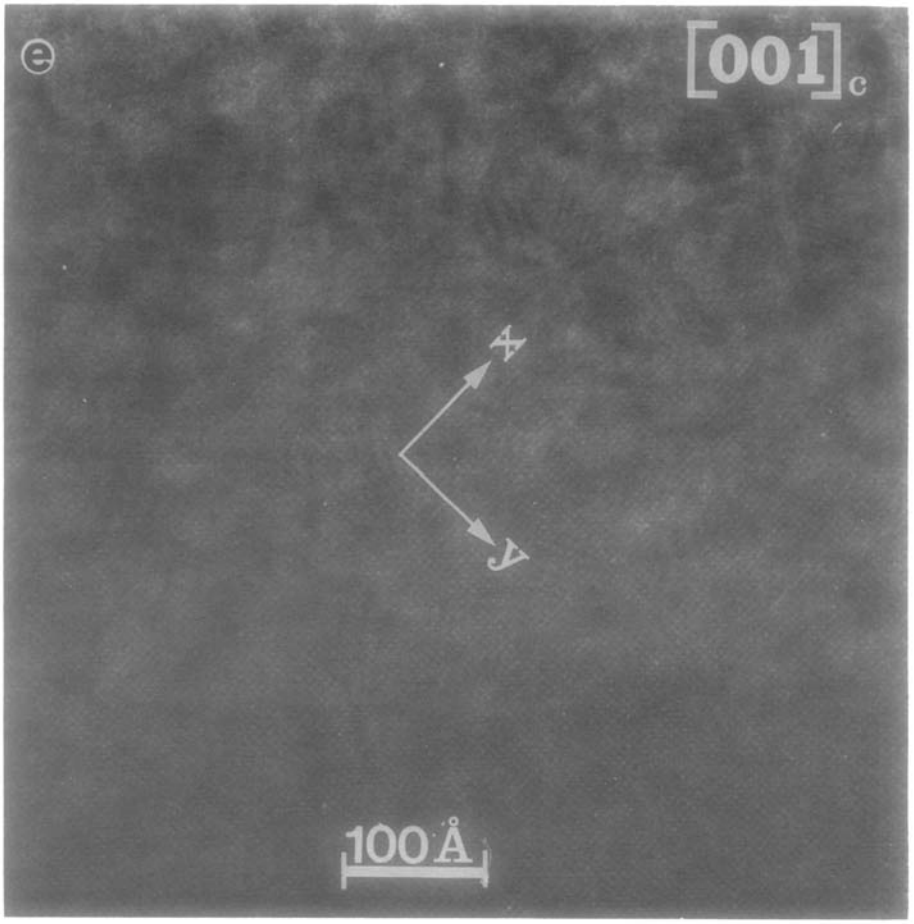

FIG. 14—*Continued*

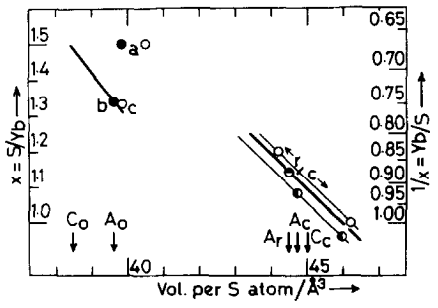

FIG. 15. Composition, x in YbS_x, versus volume per sulfur atom in the system Yb + S. ●, this work; ○, Flahaut *et al.*; ◓, Tomas *et al.*, $Yb_{0.875}S$; ◐, Eliseev *et al.* (a) Yb_2S_3, corundum type; (b) $YbS_{\sim 1.34}$; (c) Yb_3S_4.

The line in the upper left corner is that deduced in our earlier work (*6*). Of the three lines in the lower right, the right-hand one is from Flahaut *et al.* (1965) for CaS + Yb_2S_3 (rhombohedral, *r*, and cubic, *c*, B1-related $Yb_{1-\delta}S$; the two points being $Ca_{0.6}Yb_{0.4}S_{1.2}$ or $Ca_{0.5}Yb_{0.33}S$ and CaS): the left-hand one is from Eliseev *et al.* (*9*); the heavier central one is from Eliseev *et al.*, but "corrected" by us for what we deduced to be an underestimation of the sulfur content in their samples. (Note that the point of Tomas *et al.* falls exactly on this line.)

The arrows indicate volumes per S atom for our various samples, deduced from unit cell data derived from X-ray powder patterns: A, C indicate the sample (as in text); and subscripts o, r, and c indicate orthorhombic, rhombohedral, and cubic structures.

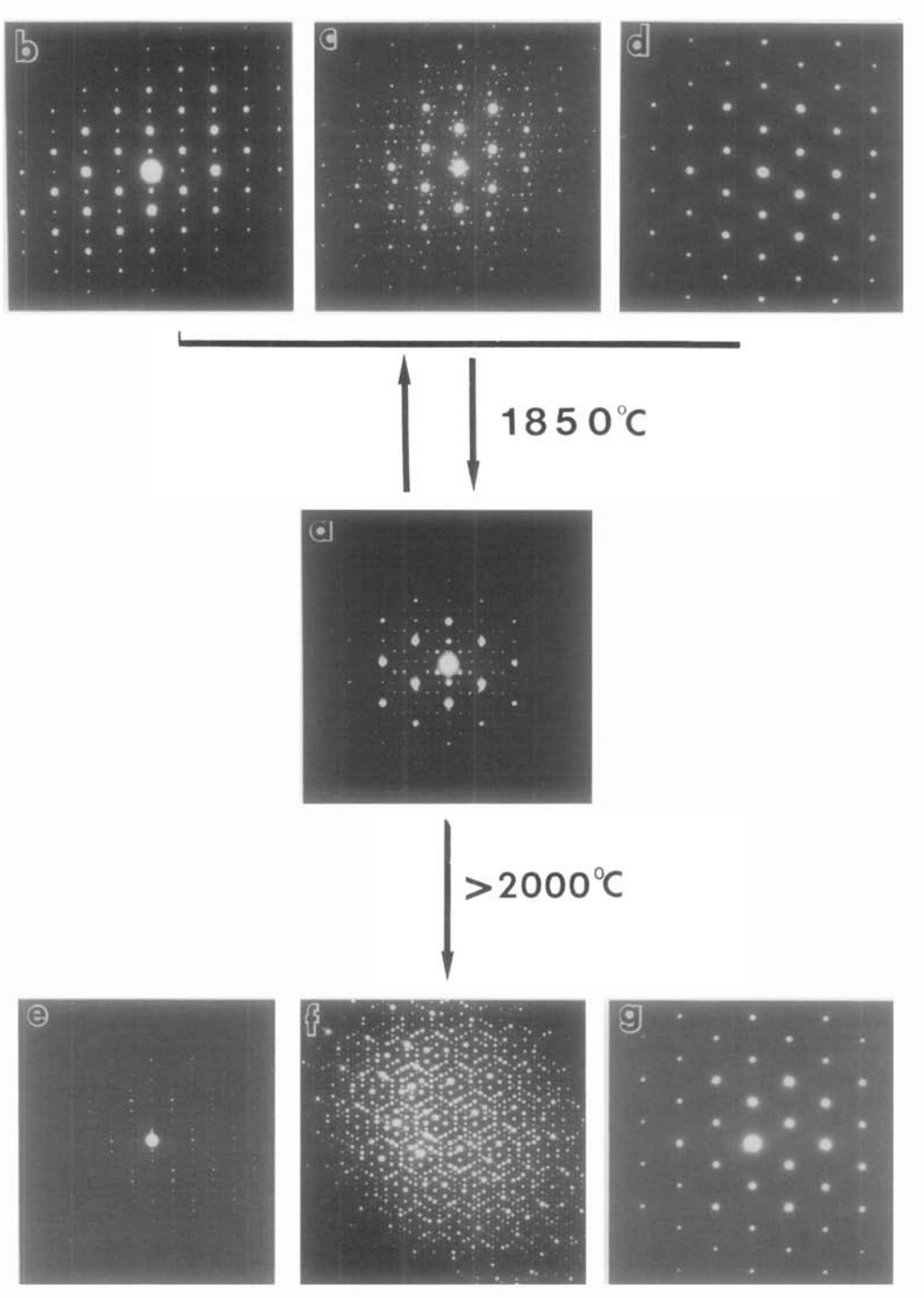

FIG. 16. Electron diffraction patterns showing the strong similarity between the arrays of Bragg reflections from the (sub-) cells of various structures observed in different samples. At the center (a) the "Yb_3S_4" starting material: a 1500°C preparation—$[001]_{Pnma}$, modulated. Above, sample A prepared at 1850°C—(b) $[001]_{Pnma}$, unmodulated; (c) $[\bar{1}10]_h = [\bar{1}2\bar{1}]_r$, modulated; (d) $[\bar{1}10]_h = [\bar{1}2\bar{1}]_r$, unmodulated. Below, sample B prepared at ≥ 2000°C—(e) $[010]_{Ccmm}$; (f) overlapping crystals of $[\bar{1}10]_h = [\bar{1}2\bar{1}]_r$; (g) $[\bar{1}10]_h = [\bar{1}2\bar{1}]_r$ untwinned and unmodulated (≡ (d)).

The transformation (a) ⇄ (b) + (c) + (d) is reversible. At $T > 2000$°C, the *Pnma* (orthorhombic) structure (a) loses its satellite reflections, and partly transforms to the *Ccmm* (also orthorhombic) structure (e).

satellites for the higher temperature *Pnma* diffraction patterns. This fits the fact that high-temperature preparations will be relatively reduced ($x = 1.33$) [and also that the 1200°C preparations (sample C) have a lower value of Δ than those made at 1500°C (*6*).]

It must be admitted that disorder, also more likely at high temperatures, would also lead to the disappearance of the satellites. However, we note that the volume per S atom for sample C (with satellites) corresponds to a stoichiometry $YbS_{1.49\pm0.01}$ (cf. Flahaut's limit of $YbS_{1.48}$), while that for sample A (no satellites) corresponds to $YbS_{1.34\pm0.03} \sim Yb_{3-\delta}S_4$ with $\delta = 0.01_5 \pm 0.02_2 \sim 0$. (cf. Fig. 15.)

(Recall also that the satellites return to the diffraction patterns when sample A is reheated in H_2S + Ar at 1500°C; cf. Fig. 16.)

Finally, we note that the *Cmcm* structure ($CaTi_2O_4$ type) is observed only in the highest temperature preparation, sample B. This is quite analogous to its observation as the high-temperature polymorph of $CaYb_2S_4$.

Rhombohedral, $Yb_{1-\delta}S$ phase. Observed only in samples A and B, the X-ray powder pattern for the latter could not be indexed satisfactorily; and so we have a unit cell volume only for A. Its volume per sulfur atom falls approximately in the region expected (for the rhombohedral phase) from Flahaut's data (*7*) for CaS + Yb_2S_3 (Fig. 15) and interestingly, it is virtually identical to that reported by Tomas *et al.* (*11*) for their sample of $Yb_{0.875}S$. However, these last authors detected no rhombohedral distortion although, as mentioned earlier, they suspected its presence. Furthermore, they observed no satellites while we are unable to determine whether or not the rhombohedral structure whose unit cell we deduced is modulated or not: both types occur in sample A.

Cubic $Yb_{1-\delta}S$ Phases. We are uncertain about our unit cell parameters in these cases. However, two cases were resolved from the X-ray powder patterns (samples A and C), and their volumes per S atom are included in Fig. 15. That for A is close to Flahaut's rhombohedral/cubic boundary (*7*); that for C is well within the cubic region.

The latter, somewhat surprisingly (for C is prepared at a lower temperature than A), corresponds to a lower ratio x = S/Yb than the former. And this might be an appropriate place to point out that, in principle at least, some oxidation (increase in sulfur content) may well occur during the cooling process (after sample preparation), so that "quenching" may be impossible, and the samples therefore inhomogeneous.

More work is necessary to resolve the behavior at lower x values, i.e., in the region of the cubic/rhombohedral phases. It seems likely (cf. the images in Figs. 10b and 14e) that fine scale disorder persists in the samples prepared at the higher temperatures (A and B), so that annealing at lower temperatures may be necessary to produce fully ordered structures.

Acknowledgments

We thank the Centro de Microscopía Electrónica (U. C. M.) for facilities. One of us, B.G.H., thanks the D.G.I.C.Y.T. (Secretaría de Estado de Universidades e Investigación, M. E. y C.) for a sabbatical visiting professorship. L.C.O.D. thanks the Australian National University (R.S.C.) for financial support.

References

1. J. Flahaut, L. Domange, M. Patrie, and M. Guittard, *C. R. Acad. Sci.* **251,** 1517 (1960).
2. J. Flahaut, L. Domange, M. Guittard, and J. Loriers, *Bull. Soc. Chim. Fr.* 102 (1961).
3. J. Flahaut, L. Domange, and M. Pardo, *C. R. Acad. Sci.* **258,** 594 (1964).
4. R. Chevalier, P. Laruelle, and J. Flahaut, *Bull. Soc. Fr. Mineral. Cristallogr.* 564 (1967).
5. M. Patrie, *Bull. Soc. Chim. Fr.* 1600 (1969).
6a. L. C. Otero-Diaz and B. G. Hyde, *Acta Crystallogr. Sect. B* **39,** 569 (1983).
6b. R. L. Withers, B. G. Hyde, A. Prodan, and F. W. Boswell, *J. Phys.: Condens. Matter* **2,** 4051 (1990).

7. M. PATRIE, J. FLAHAUT, AND L. DOMANGE, *Rev. Hautes Tempér. Réfract.* **2,** 187 (1965).
8. J. FLAHAUT, *in* "Handbook on the Physics and Chemistry of Rare Earths" (K. A. Gschneider and L. Eyring., Eds.), Vol. 4, p. 1, North-Holland, Amsterdam (1979).
9. A. A. ELISEEV, G. M. KUZ'MICHEVA, AND V. I. YASHNOV, *Russ. J. Inorg. Chem.* **23,** 273 (1978).
10. M. PATRIE, AND J. FLAHAUT, *C. R. Acad. Sci.* **264,** 395 (1967).
11. A. TOMAS, M. ROBERT, AND M. GUITTARD, *Mat. Res. Bull.* **23,** 507 (1988).
12. M. GUITTARD, J. FLAHAUT, AND L. DOMANGE, *C. R. Acad. Sci.* **262,** 1002 (1966).
13. J. A. HODGES, G. JÉHANNO, D. DEBRAY, F. HOLTZBERG, AND M. LOEWENHAUPT, *J. Phys.* **43,** 961 (1982).
14. B. G. HYDE, A. M. BAGSHAW, S. ANDERSSON, AND M. O'KEEFFE, *Annu. Rev. Mater. Sci.* **4,** 43 (1974).